Langmuir

Article

pubs.acs.org/Langmuir

van der Waals Interactions on the Mesoscale: Open-Science Implementation, Anisotropy, Retardation, and Solvent Effects

Daniel M. Dryden,[†] Jaime C. Hopkins,[#] Lin K. Denoyer,[+] Lokendra Poudel,[¶] Nicole F. Steinmetz,[†,‡,§,∥] Wai-Yim Ching,[¶] Rudolf Podgornik,[#,●,^] Adrian Parsegian,[#] and Roger H. French*[,†,∥]

[†]Department of Materials Science and Engineering, [‡]Department of Biomedical Engineering, [§]Department of Radiology, School of Medicine, [∥]Department of Macromolecular Science and Engineering, [⊥]Department of Physics, Case Western Reserve University, 10900 Euclid Avenue, Cleveland, Ohio 44106, United States

[#]Department of Physics, University of Massachusetts, Amherst, Massachusetts 01003, United States

[+]Deconvolution and Entropy Consulting, 755 Snyder Hill, Ithaca, New York 14850, United States

[¶]Department of Physics and Astronomy, University of Missouri—Kansas City, Kansas City, Missouri 64110, United States

[●]Department of Theoretical Physics, Jozef Stefan Institute, SI-1000 Ljubljana, Slovenia

[^]Department of Physics, Faculty of Mathematics and Physics, University of Ljubljana, SI-1000 Ljubljana, Slovenia

ABSTRACT: The self-assembly of heterogeneous mesoscale systems is mediated by long-range interactions, including van der Waals forces. Diverse mesoscale architectures, built of optically and morphologically anisotropic elements such as DNA, collagen, single-walled carbon nanotubes, and inorganic materials, require a tool to calculate the forces, torques, interaction energies, and Hamaker coefficients that govern assembly in such systems. The mesoscale Lifshitz theory of van der Waals interactions can accurately describe solvent and temperature effects, retardation, and optically and morphologically anisotropic materials for cylindrical and planar interaction geometries. The *Gecko Hamaker* open-science software implementation of this theory enables new and sophisticated insights into the properties of important organic/inorganic systems: interactions show an extended range of magnitudes and retardation rates, DNA interactions show an imprint of base pair composition, certain SWCNT interactions display retardation-dependent nonmonotonicity, and interactions are mapped across a range of material systems in order to facilitate rational mesoscale design.

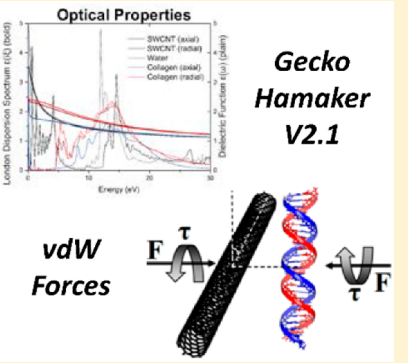

1. INTRODUCTION

The understanding, design, and control of nanoscale and mesoscale assembly presents a critical challenge across a range of disciplines.[1,2] Of particular interest for the nano-,[3] soft-,[4] and biomatter communities[5] are systems that are nanoscale in one or two dimensions but macroscopic in the remaining dimension(s),[6] such as molecular wires and ribbons,[7] single-walled carbon nanotubes (SWCNTs),[8] linear informational macromolecules, fibrous proteins, and molecular sheets including graphene,[9,10] surfactant monolayers, and biological membranes.[11] Universal in these systems are the long-range van der Waals−London dispersion (vdW) interactions[6,11] that arise from dipolar fluctuations within optically contrasting objects in an intervening medium. Existing theoretical approaches and the computational implementations of these interactions can be partitioned into the macroscopic (Lifshitz theory)[11] and microscopic (few-atom) ab initio quantum chemical[12] approaches.[13−16] The microscopic approach is particularly useful for atoms, molecules, and small clusters. The macroscopic approach is preferred for well-separated systems, where the collective response of the matter can be approximated by a frequency-dependent anisotropic dielectric function with sharp spatial boundaries at a well-defined separation, as is the case in systems with at least one macroscopic dimension. Under this condition, the vdW interaction free energy is a functional of the dielectric response $\varepsilon''(i\xi)$ at discrete thermal (Matsubara) frequencies on the imaginary frequency axis $i\xi$, which is itself a functional of the imaginary part of the dielectric response function $\varepsilon''(\omega)$ calculated via the Kramers−Kronig relations.[17,18] We have formulated a complete Lifshitz theory of vdW interactions based on the idealized planar[17,19,20] or cylindrical morphology. This facilitates the calculation of vdW interaction strengths for that interaction geometry, including the optical anisotropy of interacting materials, and accounts for retardation effects which arise from the finite propagation velocity of electromagnetic disturbances, the defining feature of the vdW interaction's separation dependence beyond the 10−100 nm regime. The effect of the solvent and its own optical dispersion can strongly influence interactions, even making them nonmonotonic with attractive and repulsive separation

Received: February 3, 2015
Revised: March 24, 2015

DOI: 10.1021/acs.langmuir.5b00106
Langmuir XXXX, XXX, XXX−XXX

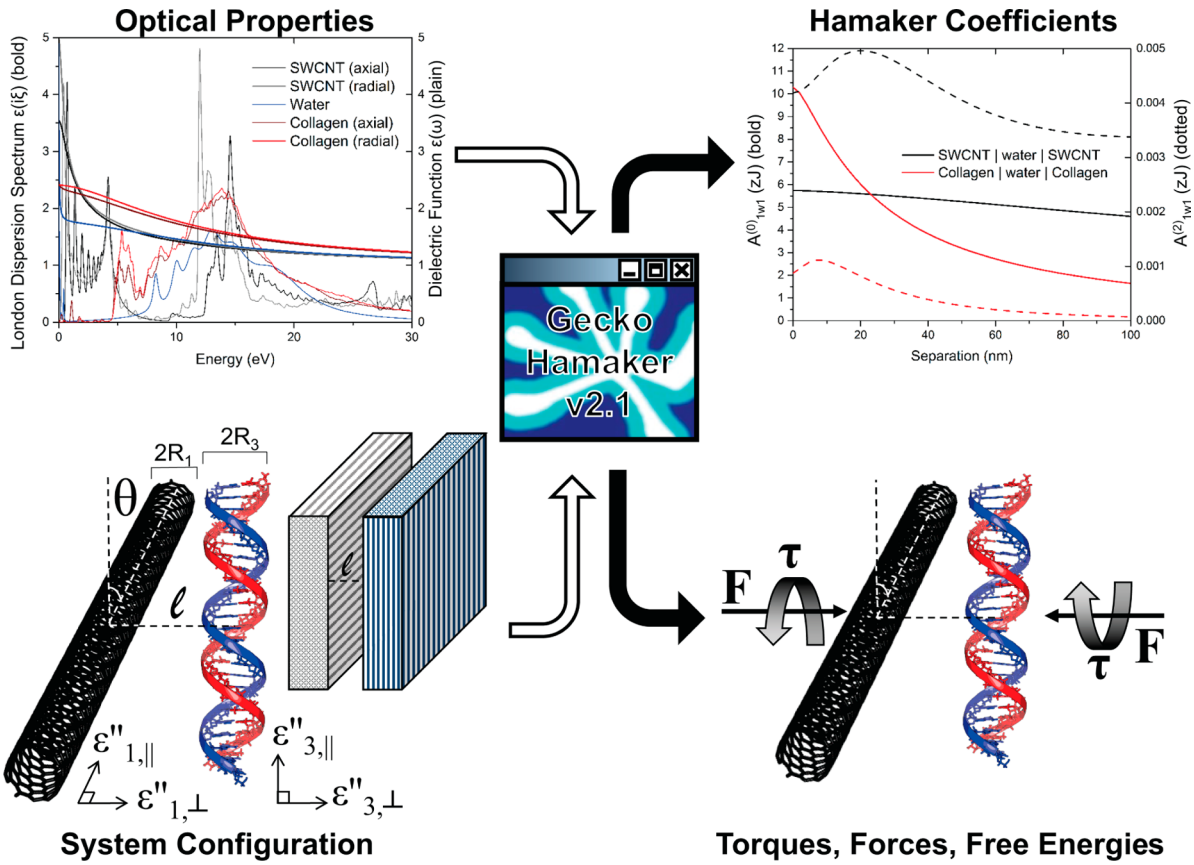

Figure 1. Schematic illustration of the *Gecko Hamaker* workflow using a large-radius (24,24,s) SWCNT and type I collagen in aqueous solvent as examples. Full spectral optical properties (upper left) are taken as input, experimentally measured using optical or electron energy-loss spectroscopy, or calculated using ab initio methods. An interaction geometry (lower left) is then chosen, consisting of optically anisotropic cylinders, optically anisotropic half-spaces, multilayered half-spaces, or graded-interface half-spaces. Specific optical properties from the spectral database are then applied to each element in the configuration. The outputs are the isotropic part $A^{(0)}{}_{1w3}$ (upper right, bold) and the anisotropic part $A^{(2)}{}_{1w3}$ of the Hamaker coefficients if applicable (upper right, dotted), as well as torques, normal forces, and thermodynamic interaction free energies (lower right). All quantities are given as functions of surface-to-surface separation l for a user-specified skew angle θ (for anisotropic systems) and radii R_1 and R_2 (for cylinders).

regimes.[15] Optical input spectra may be obtained from disparate methods, such as ab initio calculations or spectroscopic measurements.[17]

This formulation vastly improves upon previous isotropic[17] and nonretarded[8] results. We apply it to a range of technologically promising cylindrical materials, including metallic and semiconducting SWCNTs,[8,21−24] multiple composites of DNA,[25−27] collagen,[28] polystyrene,[29] and inorganic materials. Our results are presented as Hamaker coefficients, forces, and torques[30] for a wide range of symmetric (identical materials interacting across an isotropic medium) and asymmetric (different materials interacting across an isotropic medium) interaction geometries in aqueous media. We emphasize systems of general scientific interest, such as organic-silica and DNA interactions, or those that exhibit highly anomalous behavior, such as certain SWCNT interactions. This detailed formulation of the Lifshitz theory is implemented in the *Gecko Hamaker* open-source software project[31] and its optical property database (Figure 1). *Gecko Hamaker* provides a powerful open-science tool for the calculation of vdW interactions and serves the broader scientific community as a versatile assembly thermodynamics and mesoscale dynamics design tool whose applications are augmented by an ever-expanding range of materials spectra and interaction geometries. We demonstrate the versatility of *Gecko Hamaker* as a design tool for the exploration and discovery of novel features of long-range vdW interactions. We demonstrate the capabilities of *Gecko Hamaker* to calculate vdW interactions using a range of optically anisotropic cylinder examples.

2. EXPERIMENTAL SECTION

2.1. Lifshitz Theory. From measured absorption spectra and/or ab initio electronic structure calcluations, we obtain the complex dielectric function $\varepsilon(\omega) = \varepsilon'(\omega) + i\varepsilon''(\omega)$, where the imaginary part corresponds to energy dissipation in the material and vial Kramers−Kronig transform yields the London dispersion spectrum $\varepsilon(i\xi_n)$, describing the spontaneous field fluctuations at the origin of the vdW force. In the Lifshitz theory the vdW interaction is a functional of $\varepsilon(i\xi_n)$, evaluated at the discrete thermal Matsubara frequencies $\xi_n = 2\pi n k_B T/\hbar$ (n = 0, 1, ...), where k_B is the Boltzmann constant. At room temperature, Matsubara frequencies are multiples of 2.4×10^{14} Hz or 0.025 eV.

To calculate the interaction between pairs of anisotropic cylinders of materials 1 and 3, we modify the simple case of two uniaxially anisotropic planar half-spaces acting across an isotropic medium[19] by imagining the material to be composed of arrays of parallel cylinders with different anisotropic polarizabilities[8,32] and then extracting the pair interaction between uniaxial anisotropic cylinders of radii R_1 and R_3 via the Pitaevskii method.[11] The intervening space between the two arrays and the space between cylinders is assumed to be filled with an

DOI: 10.1021/acs.langmuir.5b00106
Langmuir XXXX, XXX, XXX−XXX

optically isotropic aqueous solvent of $\varepsilon_m(\omega)$ described by a single-Debye and multiple-Lorentz oscillator model.[11]

For $\varepsilon_{\parallel}^{1,3}(\omega)$, the dielectric response parallel to the longitudinal axis of the cylinder, and $\varepsilon_{\perp}^{1,3}(\omega)$, the dielectric response perpendicular to the longitudinal axis of the cylinder, we can define the relative anisotropy measures $\Delta_{\parallel}^{1,3}(\omega)$ and $\Delta_{\perp}^{1,3}(\omega)$ as

$$\Delta_{\parallel}^{1,3}(\omega) = \frac{\varepsilon_{\parallel}^{1,3}(\omega) - \varepsilon_m(\omega)}{\varepsilon_m(\omega)}, \quad \Delta_{\perp}^{1,3}(\omega) = \frac{\varepsilon_{\parallel\perp}^{1,3}(\omega) - \varepsilon_m(\omega)}{\varepsilon_{\parallel\perp}^{1,3}(\omega) - \varepsilon_m(\omega)} \tag{1}$$

The vdW interaction free energy between two semi-infinite anisotropic uniaxial dielectric layers across a finite layer of thickness l was worked out in the nonretarded limit[11] and the fully retarded limit[19] as a function of their separation l and the angle between their principal dielectric anisotropy axes θ: $G(l, \theta)$. It then follows that the interaction free energy between two cylinders, $G(l, \theta)$, whose axes are contained within the two parallel boundaries at a separation l but skewed at an angle θ is given by the second derivative $d^2G(l, \theta)/dl^2$ expanded to second order in the density of the two cylindrical arrays.[11] Note that such an expansion is possible only if the dielectric response at all frequencies is bounded so that in the case of materials with free charges one needs to model them explicitly.[33] vdW interactions between optically anisotropic cylinders acting across an isotropic medium create torques, given by

$$\tau = -\frac{dG(l, \theta)}{d\theta}$$

as well as attractions or repulsions in the normal force

$$F = -\frac{dG(l, \theta)}{dl}$$

As the separation between the bodies decreases, they feel mutual torques that favor the alignment of the principal axes. The free energy has a periodic dependence on the mutual angle, but the limit as $\theta \to 0$ has to be considered carefully as in the parallel configuration the free energy scales with the length of the cylinders.[32]

The free energy of the vdW interactions between two skewed cylinders is then obtained as

$$G_{1m3}(l, \theta) = -\frac{(\pi R_1^2)(\pi R_3^2)}{2\pi l^4 \sin\theta}(A^0_{1m3}(l) + A^2_{1m3}(l) \cos 2\theta) \tag{2}$$

where the inverse sin θ dependence stems from the shape (morphological) anisotropy and the cos 2θ dependence stems from the material anisotropy. For both symmetric and asymmetric systems with cylindrical morphology, Hamaker coefficients $A^{(0)}$ and $A^{(2)}$ are functions of separation l (Figure 1) and the ratio of relative anisotropy measures $a_{1,3}(i\xi_n)$, which depend on the material types and sampling frequencies

$$a_{1,3}(i\xi) = \frac{2\Delta_{\perp}^{1,3}(i\xi)}{\Delta_{\parallel}^{1,3}(i\xi)} \tag{3}$$

Both Hamaker coefficients are defined through a summation over the Matsubara frequencies ξ_n:

$$A^0_{1m3}(l) = \frac{k_BT}{32}\sum_{n=0}^{\infty'} \Delta_{1,\parallel}\Delta_{3,\parallel}p_n^4(l)\int_0^{\infty} t\, dt\, \frac{e^{-2p_n(l)\sqrt{t^2+1}}}{t^2+1}\tilde{g}^{(0)}(t, a_1(i\xi_n), a_3(i\xi_n)) \tag{4}$$

with

$$\tilde{g}^{(0)}(t, a_1, a_3) = 2[(1 + 3a_1)t^2 + (1 + a_1)][1 \to 3] + 4(1 + a_1)(1 + a_3)$$

and

$$A^2_{1m3}(l) = \frac{k_BT}{32}\sum_{n=0}^{\infty'} \Delta_{1,\parallel}\Delta_{3,\parallel}p_n^4(l)\int_0^{\infty} t\, dt\, \frac{e^{-2p_n(l)\sqrt{t^2+1}}}{t^2+1}\tilde{g}^{(2)}(t, a_1(i\xi_n), a_3(i\xi_n), \theta) \tag{5}$$

with

$$\tilde{g}^{(0)}(t, a_1, a_3, \theta) = (1 - a_1)(1 - a_3)(t^2 + 2)^2$$

The dimensionless factor $p_n(l) = \varepsilon_m(i\xi_n)((\xi_n^2)/(c^2))l^2$, which depends on the ratio of the travel time of light, l/c, across the intervening separation and the fluctuation lifetime, $1/\xi_n$, captures the separation dependence and retardation due to the finite speed of light. For the zero-frequency Matsubara term, the lifetime of the fluctuations is sufficiently long not to be affected by retardation.

Alternative methods for evaluating the strength of vdW interactions also exist and are robust under certain conditions. Density functional theory (DFT)-based methods[12,34] are standardly useful for atoms and small clusters, but they usually become unwieldy for systems with large numbers of electrons. However, recent advances based on fluctuating dipoles that capture both intra- and intermolecular collective fluctuations[35,36] are indeed also applicable to larger systems. Nevertheless, it is important to appreciate that the solvent effect, specifically the effect of the aqueous solvent, is crucial to many applications of vdW interactions in soft- and biomatter contexts. While the solvent effects and the related large contribution of the zero-frequency Matsubara (classical) term to the total vdW interactions both enter the Lifshitz theory "naturally" and on the same level as the fluctuation response of the interacting matter,[18] it might be quite difficult to implement them by more microscopic methods. This is the main reason that the Lifshitz theory retains its relevance in particular for soft matter- and biomatter-related problems.

For larger objects or equivalently small separations, the proximity force approximation (PFA), also referred to as the Derjaguin approximation,[15,37,38] can accurately describe objects such as colloids on the order of micrometers in radius, provided the separation between the objects is much smaller than the characteristic dimensions of the objects. However, this regime is of limited applicability for nanoscale objects where the necessary object separations would be subangstrom. The mesoscale Lifshitz theory described here in its large-separation regime is valid for mesoscale objects with separations on the nanometer scale, making it well-suited for describing realistic nano- and mesoscale interactions.

The Lifshitz theory is based on the dielectric response function and can be formulated for all the cases where this response function exists.[11] It is valid for the macroscale, mesoscale, and microscale: in fact, even the atomic pair potentials clearly follow from the application of the Pitaevskii ansatz to the general Lifshitz formula for the interaction between macroscopic bodies.[33] On this level, the question of collective fluctuations for interacting many-body aggregates enters the Lifshitz theory solely through the dielectric response function and can be fully analyzed on that level. The calculation of the latter is therefore technically not a part of the Lifshitz theory per se but has to be imported from a separate full many-body theory of the dispersion spectra. The clear decomposition into the calculation of the spectral properties and the consequent long-range vdW interaction is the principal feature of the Lifshitz theory. Thus, it is not the Lifshitz theory itself that needs to be compared or counterposed to other more microscopic theories of vdW interactions but the methodology of getting the appropriate dielectric response functions (dispersion spectra). If the full many-body dielectric response function were known in its entire time and space domain, then the Lifshitz theory would in principle be able to provide a complete and consistent description of the vdW interactions.

2.2. *Gecko Hamaker*. Recent advances in the theory of vdW interactions have facilitated the implementation of an open-source, open-data design tool that facilitates an understanding and prediction of the magnitude and properties of vdW interactions in a wide variety of contexts. The *Gecko Hamaker* open-source software project is a full implementation of the mesoscale classical Lifshitz theory for isotropic and anisotropic planar multilayer,[17] sharp, or graded interfaces for

DOI: 10.1021/acs.langmuir.5b00106
Langmuir XXXX, XXX, XXX−XXX

modeling grain boundaries[39] and cylinder−cylinder[32] interaction geometry with an intervening dielectric medium, accompanied by an extensive database of material optical properties spectra. The machine-readable optical properties database is available either for download or as a web service and makes available the full spectral properties of over 100 materials from both ab initio calculations[8,40] and experiments,[6,39,41] including inorganic as well as organic materials such as type I collagen and (GC)10 duplex DNA spectra.[40,42] The optical properties included in the database may be applied to both macro- and nanoscale objects that are macroscopic in at least one dimension such as cylinders and sheets. It is critical to note that the objects described in *Gecko Hamaker* are macroscopic in at least one dimension and furthermore that nanoscale-sized probes have in certain cases[39] been used to directly measure nanoscale optical properties, producing consistent results as inputs to the classical mesoscale Lifshitz theory. The *Gecko Hamaker* software and its source code are distributed freely on Sourceforge[31] under the GNU general public license (gnu.org). This open-science architecture is at the forefront of a growing trend, with both the U.S. government[43,44] and the G8 nations[45] emphasizing data sharing for advancing the dialogue of scientific discovery. Existing programs such as *Scuff-EM*[46] provide useful and versatile implementations for the Casimir community[6] based on user-specified geometries at zero temperature and optically isotropic systems in vacuum. *Gecko Hamaker* uses predefined geometries but allows for the calculation of temperature dependence, optical anisotropy, and variable media and provides both an existing database of material properties and a graphical user interface to increase its accessibility even to non-specialists. By making the *Gecko Hamaker* open data science tool with its spectra database freely available, we increase the opportunities for collaboration between researchers focused on long-range interactions and mesoscale design engineers in energy materials, geology, chemistry, physics, and biology.

3. RESULTS AND DISCUSSION

vdW interaction properties between different optically anisotropic materials in cylindrical interaction geometry are presented as Hamaker coeffcients, normal force, and torque (Experimental Section). The anisotropic dielectric response of the materials involved introduces two distinct Hamaker coefficients: the isotropic part, $A^{(0)}{}_{123}$, and the anisotropic part, $A^{(2)}{}_{123}$. Apart from the anisotropy of the dielectric response, the interaction free energy also contains the effects of anisotropic morphology and interaction geometry.

Within the Lifshitz formalism, the interaction free energy depends on the London dispersion spectrum $\varepsilon''(i\xi_n)$, discretely sampled at thermal Matsubara frequencies ξ_n, obtained from the Kramers−Kronig transform of $\varepsilon''(\omega)$. The latter is an input function and can be acquired by a variety of experimental and theoretical methods.[17] The *Gecko Hamaker* software platform already contains an extensive spectral database. We specifically used a combination of experimental data fits (for water)[11] and the ab initio orthogonalized linear combination of atomic orbital (OLCAO) method, explained elsewhere,[35] to calculate the electronic structure and optical properties of interacting materials. Hamaker coefficients obtained by the ab initio optical spectra for a material may sometimes differ from those calculated from an experimental spectrum of the same material. Optical contrast at different energies contributes nonuniformly to the strength of the vdW interaction;[18] as such, the bandgap underestimation that results from the local density approximation of density functional theory calculations[42] tends to skew the Hamaker coefficients. The details of this effect and strategies for its mitigation are a topic of ongoing research.[18] Apart from this caveat, it is nevertheless interesting to compare trending behavior across different methods. All interactions are evaluated in an aqueous medium (denoted by w) with the zero-frequency (static) Matsubara term completely screened,[11] assuming that the free charge carrier (salt ion) concentration in the bathing medium is sufficiently high that the zero-frequency Matsubara contribution to $A^{(0)}{}_{123}$ and $A^{(2)}{}_{123}$ vanishes (Experimental Section). This condition is met at separations of 1 nm or greater, whenever the ion concentration in the intervening medium is greater than $\sim 10^{20}$ cm^{-3}, equivalent to a univalent ion solution concentration of ~50 mM. This is a reasonable assumption for a wide range of realistic conditions, including the commonly used buffers in biological samples. The unscreened zero-frequency Matsubara term may be large in certain systems, especially those with high optical anisotropy at low frequencies, e.g., all systems involving an aqueous medium but also metallic SWCNTs, where the chiral indices[8] (n, m) are such that $(n - m)/3$ = integer. For amorphous SiO_2, the zero-frequency contribution to $A^{(0)}{}_{1w1}$ is 2.15 zJ; by comparison, for the (5,2,m) metallic SWCNT it is 50.5 zJ. This screening effect may be most significant for materials with a small dielectric contrast at all energies. For these materials, screening out the relatively large zero-frequency contribution can result in a large change in the free energy as well as increase the weighting of contributions from medium and high energies. Here we observe that the static contribution for the (5,2,m) SWCNT, while large, accounts for only 4.4% of the interaction strength in that system; for aSiO_2, the zero-frequency term accounts for 24.8% of the interaction strength. For idealized metallic systems in vacuo, without any screening of the zero-frequency term, the low-temperature vdW interactions would converge to Casimir forces,[13] a case we do not analyze here.[15] Wherever the isotropic and anisotropic Hamaker coefficients are discussed as single values, the surface-to-surface separation between idealized cylinders is taken to be 5 nm. At this spacing, retardation can have a noticeable effect on the high energy contributions to the summation terms of the Hamaker coefficients, but the low-energy contributions tend to remain unaffected.

3.1. Range of Magnitudes. The $A^{(0)}{}_{1w1}(l)$ and the $A^{(2)}{}_{1w1}(l)$ Hamaker coefficients for cylindrical bodies may take on a wide range of values in symmetric systems (denoted 1w1), where both cylinders consist of the same material (Figure 2). The largest $A^{(0)}{}_{1w1}(l)$ value seen are for metallic SWCNTs,

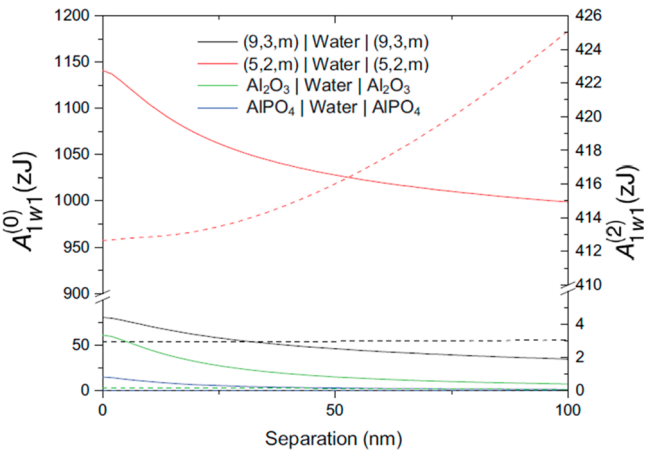

Figure 2. Range of magnitudes for symmetric configuration $A^{(0)}{}_{1w1}$ isotropic (solid lines) and anisotropic $A^{(2)}{}_{1w3}$ (dotted lines) cylindrical Hamaker coefficients for the fully retarded formulation, with the zero-frequency contribution screened in the intervening aqueous medium.

DOI: 10.1021/acs.langmuir.5b00106
Langmuir XXXX, XXX, XXX−XXX

including the chiralities (5,2,m) and (9,3,m). Hamaker coefficients for SWCNTs are consistent with those published previously,[8] and (5,2,m), because of its high optical anisotropy, exhibits an $A^{(0)}{}_{1w1}(l)$ value an order of magnitude larger than any other material studied here. Inorganic ceramics such as Al_2O_3 and $AlPO_4$ but also fibrous proteins such as type I collagen tend to exhibit substantial Hamaker coefficients. In general, materials with a lower optical contrast with water tend to exhibit smaller Hamaker coefficients, as observed for DNA, large-radius SWCNTs such as(24,24,s), $aSiO_2$, and polystyrene (Figure 3). While Hamaker coefficients for various types of

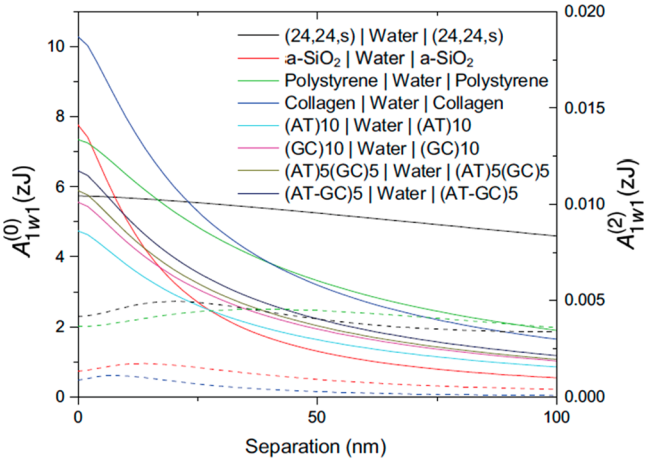

Figure 3. Symmetric configuration isotropic $A^{(0)}{}_{1w1}$ (solid lines) and anisotropic $A^{(2)}{}_{1w1}$ (dotted lines) Hamaker coefficients for cylindrical morphology in the fully retarded formulation with a screened zero-frequency contribution in the case of an intervening aqueous medium. All materials here, including all biomaterials included in this study, have $A^{(0)}{}_{1w1} < 10$ zJ.

DNA molecules are comparatively smaller, they do depend on the base-pair sequence details and could control the finer details of the equilibrium assembly structure.

3.2. Retardation Effects. The effect of retardation is seen in the rate of change of $A^{(0)}{}_{1w1}(l)$ with separation. It is strongly material-dependent and is due to the finite speed of light across the intervening medium, dephasing the correlated fluuctuations with small lifetimes, i.e., high frequencies. The high-frequency contributions to the optical contrast in a system vary with the particular London dispersion spectrum $\varepsilon(i\xi)$ for each material.[11] If the vdW interaction within a particular system results primarily from high-frequency contributions, such a system will exhibit a faster rate of retardation than a system where the interaction results from lower-frequency optical contrast. The (24,24,s) SWCNT (Figure 3, black) does not have a particularly large $A^{(0)}{}_{1w1}(l)$ at small separations, but it exhibits little retardation. Thus, its Hamaker coeffcient for ∼50 nm becomes by far the largest in this set. The majority of its optical contrast with water occurs at low frequencies; it is thus relatively impervious to retardation (optical properties inset, Figure 1). In contrast, type I collagen (Figure 3, blue) has its optical contrast with water spread out over a wide range of frequencies, including a significant contribution from high-energy Matsubara frequencies. Because of this, it exhibits dramatic retardation because these frequencies rapidly dephase with increasing separation. Under certain conditions, the effects of retardation can lead to a change of sign in the Hamaker coefficients as a function of separation, as observed previously in other systems.[32,47]

3.3. Angular Dependence. The vdW interaction free energy depends on the mutual angle between interacting cylinders in two ways (Experimental Section): the anisotropic shape of the cylinders and the anisotropic dielectric response of the cylinder material. Because of the extreme anisotropy of the cylindrical shape, the interaction free energy shows an overall $1/\sin(\theta)$ dependence on the mutual orientation of their axes as they rotate from an aligned to a perpendicular configuration. In addition, anisotropies in material dielectric responses lead to two Hamaker coeffcients, $A^{(0)}$ and $A^{(2)}$, with the second one weighted by a $\cos(2\theta)$ angular dependence. In general, the magnitude of $A^{(0)}$ is much larger than that of $A^{(2)}$, so $A^{(0)}$ dominates the angular dependence and sign of the free energy and torque. Anisotropic Hamaker coefficient $A^{(2)}{}_{1w1}$ for cylindrical morphology, which describes the dependence of the Hamaker coefficient on the skew angle θ between the cylinders, shows an unusual nonmonotonic dependence on separation (Figures 2 and 3). Unlike $A^{(0)}{}_{1w1}$, which in general tends to decrease monotonically, $A^{(2)}{}_{1w1}$ exhibits a pronounced local maximum at separations ranging from a few nanometers to a few hundred nanometers, suggesting that vdW interactions in some systems may have a more pronounced angular dependence within a certain regime of separations. In general, $A^{(0)}{}_{1w1}$ has a complex dependence on the optical (parallel and perpendicular response) anisotropy in the system. The nonmonotonic retardation effect is seen even in materials with no optical anisotropy, e.g., $aSiO_2$, indicating the geometric anisotropy as its primary source; the magnitude of the effect and the position of the maximum of the anisotropic Hamaker coefficient are nonetheless modified by the particular nature of the material's optical properties and optical anisotropy. As with the $A^{(0)}{}_{1w1}$, $A^{(2)}{}_{1w1}$ also varies drastically for different materials, with a strong correlation with the degree of optical anisotropy in the material. (AT)10 DNA has an $A^{(2)}{}_{1w1}$ that is effectively zero, even at small separations, indicating that the contribution of optical anisotropy may be quite small in such systems. Conversely, metallic SWCNTs have a large optical anisotropy and subsequently exhibit anomalously high $A^{(2)}{}_{1w1}$ values, as large as 33.6 zJ for (5,2,m) SWCNTs (Figure 3). Even the (24,24,s) SWCNT, which has a relatively modest value of $A^{(0)}{}_{1w1}$ at small separations, has an $A^{(2)}{}_{1w1}$ that is an order of magnitude larger than for less-anisotropic materials with comparable $A^{(0)}{}_{1w1}$ values (Figure 3).

3.4. Asymmetric Systems. Understanding the interactions in asymmetric systems, where materials 1 and 3 differ, is paramount for mesoscale system design. A particularly relevant case for applications in sensors[48] and nanobio interfaces[5] is the vdW interaction of biomaterials with silica nanorods (Figure 4). Silica's interaction with collagen results in a Hamaker coefficient that is 39% larger than that of the silica−(GC)10 DNA interaction at 5 nm separation. However, both interactions are strongly diminished by retardation effects compared to the silica-(24,24,s) SWCNT interaction. This phenomenon is tied to the details of the particular optical spectra that in turn govern the details of the retardation screening. The values of $A^{(2)}{}_{1w1}(l)$ clearly exhibit a more complex nonmonotonicity than that observed in symmetric systems; this effect is discussed in detail below. In some cases (not shown here), the dielectric responses of materials allow for a repulsive interaction, i.e., a negative Hamaker coefficient.[32,47] Consequently, this implies that torques also have a sign

DOI: 10.1021/acs.langmuir.5b00106
Langmuir XXXX, XXX, XXX−XXX

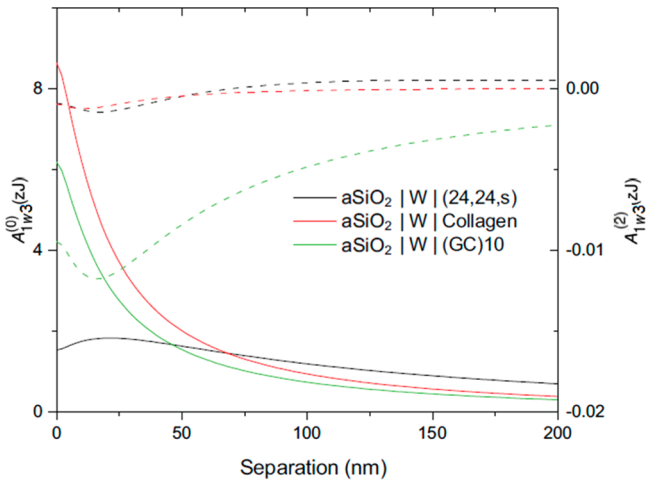

Figure 4. Asymmetric configuration $A^{(0)}{}_{1w3}$ (solid lines) and $A^{(2)}{}_{1w3}$ (dotted lines) cylindrical Hamaker coefficients for the interaction of silica nanorods with biological materials in the fully retarded formulation with a screened zero-frequency contribution for an intervening aqueous medium.

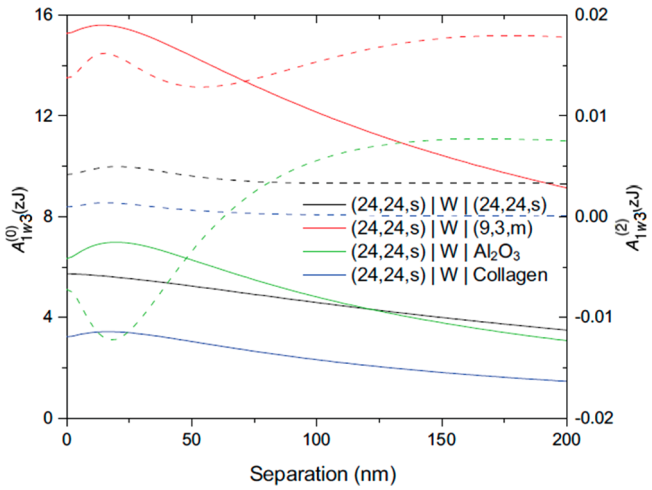

Figure 5. Asymmetric configuration $A^{(0)}{}_{1w3}$ (solid lines) and anisotropic $A^{(2)}{}_{1w3}$ (dotted lines) cylindrical Hamaker coefficients for the interaction of silica nanorods with biological materials in the fully retarded formulation with a screened zero-frequency contribution in the case of an intervening aqueous medium.

opposite to that of attractive interaction cases. If for illustration purposes we compare the symmetric system (9,3,m)-Al_2O_3-(9,3,m) with asymmetric system (9,3,m)-Al_2O_3-GC(10), we see that indeed the torque as well as the force change sign. This means that in the first case the two cylinders would tend to align whereas in the second case they will tend to assume a perpendicular configuration.

3.5. Nonmonotonicity. Nonmonotonic Hamaker coefficients may be observed in asymmetric systems.

When the dielectric functions in a planar system change in a stepwise manner, i.e., $\varepsilon(i\xi)_1 > \varepsilon(i\xi)_w > \varepsilon(i\xi)_3$, the contribution at those Matsubara frequencies $i\xi$ where the stepwise condition is met adds a repulsive element to the overall vdW interaction. This can lead to a range of effects including nonmonotonic values of $A^{(0)}{}_{1w3}$, leading to a minimum in the interaction energy or even overall net repulsive interactions.[47] In cylindrical systems with anisotropic dielectric responses, however, this condition is significantly more complicated because of the intertwined morphological and optical anisotropy of the cylinders, the latter a consequence of different axial and radial components of the dielectric responses.[32] Nevertheless, similar effects on the sign of the force may be observed as well as on the sign of torque. The Hamaker coefficients for a (24,24,s) SWCNT interacting with a range of different materials (Figure 5) show a nonmonotonic dependence on spacing l for all asymmetric systems shown here, wherein $A^{(0)}{}_{1w3}$ first rises before falling again. This complex dependence may be readily explained by observing the nature of the optical contrast in the system. For the ((24,24,s)|w|collagen) system, the optical properties $\varepsilon(i\xi)$ (Figure 1, optical properties inset) show a clear stepwise nature at energies above 10 eV, leading to repulsive contributions from the high-energy Matsubara frequencies. As these energies are gradually screened out by retardation, they no longer contribute repulsive terms to the interaction, leading to a net increase in $A^{(0)}{}_{1w3}$. At sufficiently large spacings, even the attractive low-energy contributions are damped by retardation, implying a decrease in $A^{(0)}{}_{1w3}$ as spacing tends towards infinity. The asymmetric Hamaker coefficients, though small, show an even more complex dependence on the separation, with $A^{(2)}{}_{1w3}$ showing the same small-separation local maximum, followed by another gradual rise at larger separations. Under certain circumstances, including the (24,24,s)|w|(Al_2O_3) system (green), $A^{(2)}{}_{1w3}$ shows a negative-to-positive transition, indicating that increasing alignment between the nanotubes may either increase or decrease the interaction strength depending on the cylinder−cylinder separation. This effect has never been observed or discussed in other systems and would not be predicted by more simplistic approaches to vdW interactions that ignore either optical anisotropy or retardation effects.

3.6. Hamaker Coefficient Data Mining. The true versatility of the *Gecko Hamaker* software platform implementing the Lifshitz theory of vdW interactions is particularly evident when considering systems with a wide range of materials with disparate optical properties. Instead of calculating the interaction characteristics of a single material pair, the software facilitates the exploration of arrays of systems to seek out the desired properties in order to guide material selection and configuration (Figure 6). A number of trends are immediately discernible. Torques and normal forces, which depend on both Hamaker coefficients, show a strong dependence on the cylinder radius as well as on the details of the spectral properties of the interacting materials (Figure 6, inset). This is evident in the case of interactions involving the (24,24,s) SWCNT that show large torques and normal forces in spite of their modest Hamaker coefficients, whereas small-radius SWCNTs exhibit large values of $A^{(0)}{}_{1w3}$ and $A^{(2)}{}_{1w3}$ but smaller torques. Nevertheless, in all systems investigated there exists a strong normal force and a modest but always present torque seeking to align the cylinders. Al_2O_3 interactions with other inorganics tend to have disproportionately large torques despite their relatively modest Hamaker coefficients and radii. Through data mining the Hamaker coefficients, the full power of *Gecko Hamaker* as a cross-system design platform comes to the forefront: by analyzing across many different materials, one may seek the interaction properties that are desired and subsequently will be inspired to use materials that had not been previously considered. Despite the power and versatility of the *Gecko Hamaker* software platform, user interpretation of the results is paramount. Hamaker coefficients express the material-

DOI: 10.1021/acs.langmuir.5b00106
Langmuir XXXX, XXX, XXX−XXX

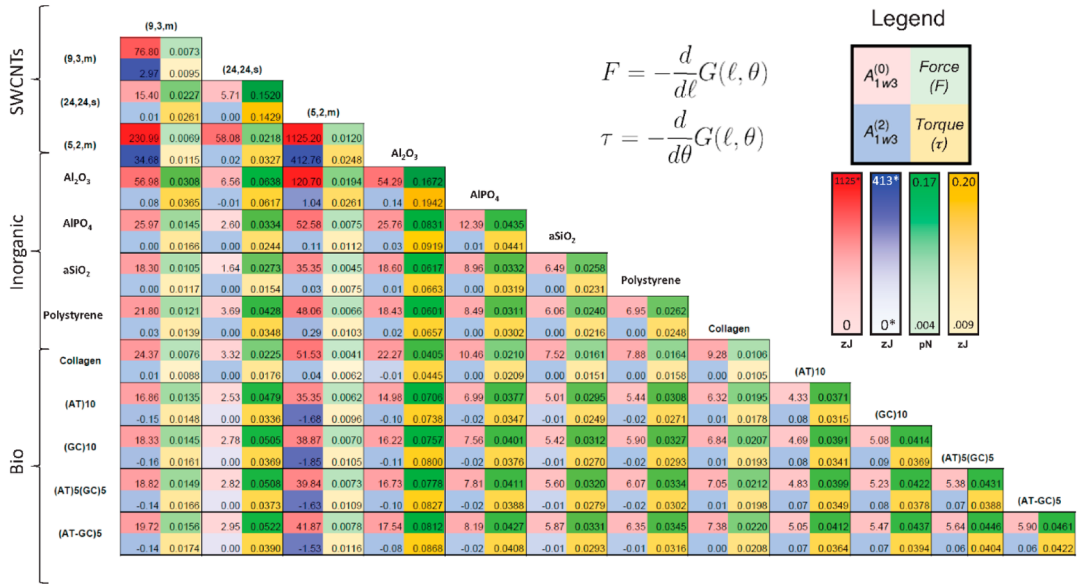

Figure 6. Pairs plot of symmetric and asymmetric interactions of anisotropic cylinders across an aqueous medium. The Hamaker coefficients, $A^{(0)}_{1w3}$ and $A^{(2)}_{1w3}$, and the forces and torques at a skew angle of 45°, at l = 5 nm separation are shown for interactions between a wide array of different materials, including biological materials, canonical inorganic materials, and SWCNTs. Cells are shaded according to interaction energy magnitudes. Torques and forces are calculated using commonly accepted literature values for radii of SWCNTs and biomaterials and a 1 nm radius for all other materials. The asterisk indicates that the color scale for $A^{(0)}_{1w3}$ saturates at 121 zJ for clarity and for $A^{(2)}_{1w3}$ saturates at 3.0 zJ, with negative values shaded according to their absolute value.

dependent nuances of the vdW interaction, but they are not equivalent to the interaction free energy itself, which has a separate dependence on cylinder radii, skew angle, and separation of its own. Effects such as retardation are therefore superimposed on these trends in the separation dependence of $A^{(0)}_{1w3}$ and $A^{(2)}_{1w3}$. As such, even when $A^{(2)}_{1w3}$ increases with separation, the net free energy of interaction may nonetheless monotonically decrease. It is important that these features of the Hamaker coefficients be properly interpreted and used for each particular application.

4. CONCLUSIONS

The mesoscale Lifshitz theory of vdW interactions has reached a level of refinement where it allows consistent and complete inclusion of solvent and temperature effects, retardation, optical anisotropy, morphology of interacting bodies, and geometry of interaction. In the limit of infinite area planar and infinitely long cylinder interaction geometries, it yields a full numerical implementation encoded in the *Gecko Hamaker* open-science software tool. The *Gecko Hamaker* software tool integrates a web service for the distribution of detailed optical properties of a broad range of heterogeneous functional materials from the spectral database and the newly implemented analytical solutions to the Lifshitz theory for a range of isotropic and anisotropic system configurations, yielding Hamaker coefficients along with torques, forces, and free energies (Figure 1). The calculated Hamaker coefficients for cylindrical interaction geometry may vary by a few orders of magnitude, depending on the materials involved in the systems, with inorganic materials generally having larger Hamaker coefficients and biomolecular materials exhibiting smaller ones. The angular dependence of the vdW interaction, depending directly on the shape anisotropy and indirectly on the optical property anisotropy through the anisotropic part of the Hamaker coefficient, also varies significantly between materials. Both $A^{(0)}_{1w3}$ and $A^{(2)}_{1w3}$ in fact exhibit dramatic and nonmonotonic retardation effects, which vary significantly depending on the high-frequency contributions to the optical mismatch in a given system and are responsible for a wide array of interesting and unexpected effects. In addition, asymmetric systems may exhibit non-monotonic Hamaker coefficients, with distinct characteristics leading to novel and controllable design paradigms. What is important is the interconnectedness of all of these effects that precludes simple approximation schemes that focus on one or the other but misses the important links between them. The present mesoscale formulation of the classical Lifshitz theory of vdW interactions, taking fully into account the retardation as well as the anisotropy of interacting materials, constitutes a significant advance in accuracy and predictive power for the computation of vdW interactions compared to previous implementations of nonretarded, isotropic solutions. Furthermore, the calculations accessible via the *Gecko Hamaker* open-science software tool may provide useful guidance to application engineers in streamlining the process of calculating appropriate Hamaker coefficients, eliminating the need for rough and misleading approximations, and making available optical properties of a wide variety of functional materials. This will allow a detailed investigation of the long-range interactions between materials and the design of specific model systems.

AUTHOR INFORMATION

Corresponding Author

*E-mail: rxf131@case.edu.

Author Contributions

The manuscript was written through the contributions of all authors. All authors have given approval to the final version of the manuscript.

Notes

The authors declare no competing financial interest.

DOI: 10.1021/acs.langmuir.5b00106
Langmuir XXXX, XXX, XXX−XXX

■ ACKNOWLEDGMENTS

This research was supported by the U.S. Department of Energy, Office of Basic Energy Sciences, Division of Materials Sciences and Engineering under awards DE-SC0008176 and DE-SC0008068. W.Y.C. thanks the National Energy Research Scientific Computing Center, a DOE Office of Science User Facility supported by the Office of Science of the U.S. Department of Energy under contract no. DE-AC03-76SF00098.

■ REFERENCES

(1) Ninham, B. W.; Nostro, P. L. *Molecular Forces and Self Assembly*; Cambridge University Press, 2011.
(2) Min, Y.; Akbulut, M.; Kristiansen, K.; Golan, Y.; Israelachvili, J. The Role of Interparticle and External Forces in Nanoparticle Assembly. *Nat. Mater.* **2013**, *7*, 527−538.
(3) Bishop, K. J. M.; Wilmer, C. E.; Soh, S.; Grzybowski, B. A. Nanoscale Forces and Their Uses in Self-Assembly. *Small* **2009**, *5*, 1600−1630.
(4) Frenkel, D.; Wales, D. J. Colloidal Self-Assembly: Designed to Yield. *Nat. Mater.* **2011**, *10*, 410−411.
(5) Nel, A. E.; Maedler, L.; Velegol, D.; Xia, T.; Hoek, E. M. V.; Somasundaran, P.; Klaessig, F.; Castranova, V.; Thompson, M. Understanding Biophysicochemical Interactions at the Nanobio Interface. *Nat. Mater.* **2009**, *8*, 543−557.
(6) French, R.; Parsegian, V.; Podgornik, R.; Rajter, R.; Jagota, A.; Luo, J.; Asthagiri, D.; Chaudhury, M.; Chiang, Y.; Granick, S.; et al. Long Range Interactions in Nanoscale Science. *Rev. Mod. Phys.* **2010**, *82*, 1887−1944.
(7) Drosdoff, D.; Woods, L. M. Quantum and Thermal Dispersion Forces: Application to Graphene Nanoribbons. *Phys. Rev. Lett.* **2014**, *112*, 025501.
(8) Rajter, R. F.; French, R. H.; Ching, W. Y.; Podgornik, R.; Parsegian, V. A. Chirality-Dependent Properties of Carbon Nanotubes: Electronic Structure, Optical Dispersion Properties, Hamaker Coefficients and van Der Waals-London Dispersion Interactions. *RSC Adv.* **2013**, *3*, 823−842.
(9) Shih, C.-J.; Strano, M. S.; Blankschtein, D. Wetting Translucency of Graphene. *Nat. Mater.* **2013**, *12*, 866−869.
(10) Geim, A. K.; Grigorieva, I. V. Van Der Waals Heterostructures. *Nature* **2011**, *499*, 419−425.
(11) Parsegian, V. A. *Van Der Waals Forces: A Handbook for Biologists, Chemists, Engineers, and Physicists*; Cambridge University Press, 2006.
(12) Klimes, J.; Michaelides, A. Perspective: Advances and Challenges in Treating van Der Waals Dispersion Forces in Density Functional Theory. *J. Chem. Phys.* **2012**, *137*, 120901−120912.
(13) Emig, T. Casimir Physics: Geometry, Shape and Material. *J. Mod. Phys. A* **2010**, *25*, 2177−2195.
(14) Dalvit, D.; Milonni, P.; Roberts, D.; Rosa, F. *Casimir Physics*; Springer, 2011.
(15) Rodriguez, A. W.; Capasso, F.; Johnson, S. G. The Casimir Effect in Microstructured Geometries. *Nat. Photonics* **2011**, *5*, 211−221.
(16) Gobre, V. V.; Tkatchenko, A. Scaling Laws for van Der Waals Interactions in Nanostructured Materials. *Nat. Commun.* **2013**, *4*, 2341−2346.
(17) French, R. H. Origins and Applications of London Dispersion Forces and Hamaker Constants in Ceramics. *J. Am. Ceram. Soc.* **2000**, *83*, 2117−2146.
(18) Hopkins, J. C.; Dryden, D. M.; Ching, W.-Y.; French, R. H.; Parsegian, V. A.; Podgornik, R. Dielectric Response Variation and the Strength of van Der Waals Interactions. *J. Colloid Interface Sci.* **2014**, *417*, 278−284.
(19) Munday, J. N.; Iannuzzi, D.; Barash, Y.; Capasso, F. Torque on Birefringent Plates Induced by Quantum Fluctuations. *Phys. Rev. A* **2005**, *71*, 042102.
(20) Narayanaswamy, A.; Zheng, Y. Van Der Waals Energy and Pressure in Dissipative Media: Fluctuational Electrodynamics and Mode Summation. *Phys. Rev. A* **2013**, *88*, 012502.
(21) Warner, J. H.; Young, N. P.; Kirkland, A. I.; Briggs, G. A. D. Resolving Strain in Carbon Nanotubes at the Atomic Level. *Nat. Mater.* **2011**, *10*, 958−962.
(22) Strano, M. S.; Jain, R. M.; Tvrdy, K.; Han, R.; Ulissi, Z. W. A Quantitative Theory of Adsorptive Separation for the Electronic Sorting of Single-Walled Carbon Nanotubes. *ACS Nano* **2014**, 3367−3379.
(23) Srivastava, A.; Srivastava, O. N.; Talapatra, S.; Vajtai, R.; Ajayan, P. M. Carbon Nanotube Filters. *Nat. Mater.* **2004**, *3*, 610−614.
(24) Sethi, S.; Ge, L.; Ci, L.; Ajayan, P. M.; Dhinojwala, A. Gecko-Inspired Carbon Nanotube-Based Self-Cleaning Adhesives. *Nano Lett.* **2008**, *8*, 822−825.
(25) Zheng, J.; Birktoft, J. J.; Chen, Y.; Wang, T.; Sha, R.; Constantinou, P. E.; Ginell, S. L.; Mao, C.; Seeman, N. C. From Molecular to Macroscopic via the Rational Design of a Self-Assembled 3D DNA Crystal. *Nature* **2009**, *461*, 74−77.
(26) Young, K. L.; Ross, M. B.; Blaber, M. G.; Rycenga, M.; Jones, M. R.; Zhang, C.; Senesi, A. J.; Lee, B.; Schatz, G. C.; Mirkin, C. A. Using DNA to Design Plasmonic Metamaterials with Tunable Optical Properties. *Adv. Mater.* **2014**, *26*, 653−659.
(27) Liu, N.; Hentschel, M.; Weiss, T.; Alivisatos, A. P.; Giessen, H. Three-Dimensional Plasmon Rulers. *Science* **2011**, *332*, 1407−1410.
(28) Cheng, X.; Gurkan, U. A.; Dehen, C. J.; Tate, M. P.; Hillhouse, H. W.; Simpson, G. J.; Akkus, O. An Electrochemical Fabrication Process for the Assembly of Anisotropically Oriented Collagen Bundles. *Biomaterials* **2008**, *29*, 3278−3288.
(29) Jin, M.; Feng, X.; Feng, L.; Sun, T.; Zhai, J.; Li, T.; Jiang, L. Superhydrophobic Aligned Polystyrene Nanotube Films with High Adhesive Force. *Adv. Mater.* **2005**, *17*, 1977−1981.
(30) Capasso, F.; Munday, J. N.; Iannuzzi, D.; Chan, H. B. Casimir Forces and Quantum Electrodynamical Torques: Physics and Nanomechanics. *IEEE J. Sel. Top. Quantum Electron.* **2007**, *13*, 400−414.
(31) *Gecko Hamaker*; 2014.
(32) Siber, A.; Rajter, R.; French, R.; Ching, W.; Parsegian, V.; Podgornik, R. Dispersion Interactions between Optically Anisotropic Cylinders at All Separations: Retardation Effects for Insulating and Semiconducting Single-Wall Carbon Nanotubes. *Phys. Rev. B* **2009**, *80*, 165414.
(33) Pitaevskii, L. P. Thermal Lifshitz Force between an Atom and a Conductor with a Small Density of Carriers. *Phys. Rev. Lett.* **2008**, *101*, 163202.
(34) Dobson, J. F.; Gould, T. Calculation of Dispersion Energies. *J. Phys.: Condens. Matter* **2012**, *24*, 073201.
(35) Tkatchenko, A. Current Understanding of Van Der Waals Effects in Realistic Materials. *Adv. Funct. Mater.* **2014**, n/a−n/a.
(36) Jr, R. A. D.; Gobre, V. V.; Tkatchenko, A. Many-Body van Der Waals Interactions in Molecules and Condensed Matter. *J. Phys.: Condens. Matter* **2014**, *26*, 213202.
(37) Zhao, R.; Luo, Y.; Fernández-Domínguez, A. I.; Pendry, J. B. Description of van Der Waals Interactions Using Transformation Optics. *Phys. Rev. Lett.* **2013**, *111*, 033602.
(38) Argento, C.; Jagota, A.; Carter, W. C. Surface Formulation for Molecular Interactions of Macroscopic Bodies. *J. Mech. Phys. Solids* **1997**, *45*, 1161−1183.
(39) Van Benthem, K.; Tan, G.; French, R. H.; DeNoyer, L. K.; Podgornik, R.; Parsegian, V. A. Graded Interface Models for More Accurate Determination of van Der Waals−London Dispersion Interactions across Grain Boundaries. *Phys. Rev. B* **2006**, *74*, 205110.
(40) Poudel, L.; Rulis, P.; Liang, L.; Ching, W.-Y. Partial Charge and Hydrogen Bonding in Four Periodic B-DNA Models. *Phys. Rev. E* **2014**, 2705−2705.
(41) French, R.; Mullejans, H.; Jones, D.; Duscher, G.; Cannon, R.; Ruhle, M. Dispersion Forces and Hamaker Constants for Intergranular Films in Silicon Nitride from Spatially Resolved-Valence Electron Energy Loss Spectrum Imaging. *Acta Mater.* **1998**, *46*, 2271−2287.

DOI: 10.1021/acs.langmuir.5b00106
Langmuir XXXX, XXX, XXX−XXX

709 (42) Ching, W.-Y.; Rulis, P. *Electronic Structure Methods for Complex*
710 *Materials: The Orthogonalized Linear Combination of Atomic Orbitals*;
711 Oxford University Press, 2012.
712 (43) Holdren, J. P. *Increasing Access to the Results of Federally Funded*
713 *Scientific Research*; Executive Office of the President: Office of Science
714 and Technology Policy, 2013.
715 (44) ObamaB. H.*Executive Order − Making Open and Machine*
716 *Readable the New Default for Government Information*; 2013.
717 (45) Open Data Charter; https://www.gov.uk/government/
718 publications/open-Data-Charter, 2013.
719 (46) Homer ReidM. T.JohnsonS. G.Efficient Computation of Power,
720 Force, and Torque in BEM Scattering Calculations. *arXiv:1307.2966*,
721 **2013**.
722 (47) Elbaum, M.; Schick, M. Application of the Theory of Dispersion
723 Forces to the Surface Melting of Ice. *Phys. Rev. Lett.* **1991**, *66*, 1713−
724 1716.
725 (48) Zhang, G.-J.; Zhang, G.; Chua, J. H.; Chee, R.-E.; Wong, E. H.;
726 Agarwal, A.; Buddharaju, K. D.; Singh, N.; Gao, Z.; Balasubramanian,
727 N. DNA Sensing by Silicon Nanowire: Charge Layer Distance
728 Dependence. *Nano Lett.* **2008**, *8*, 1066−1070.

DOI: 10.1021/acs.langmuir.5b00106
Langmuir XXXX, XXX, XXX−XXX